Kidney-Targeted Birt-Hogg-Dubé Gene Inactivation in a Mouse Model: Erk1/2 and Akt-mTOR Activation, Cell Hyperproliferation, and Polycystic Kidneys

Masaya Baba, Mutsuo Furihata, Seung-Beom Hong, Lino Tessarollo, Diana C. Haines, Eileen Southon, Vishal Patel, Peter Igarashi, W. Gregory Alvord, Robert Leighty, Masahiro Yao, Marcelino Bernardo, Lilia Ileva, Peter Choyke, Michelle B. Warren, Berton Zbar, W. Marston Linehan, Laura S. Schmidt

Background Patients with Birt-Hogg-Dubé (BHD) syndrome harbor germline mutations in the *BHD* tumor suppressor gene that are associated with an increased risk for kidney cancer. *BHD* encodes folliculin, a protein that may interact with the energy- and nutrient-sensing 5′-AMP-activated protein kinase-mammalian target of rapamycin (AMPK-mTOR) signaling pathways.

Methods We used recombineering methods to generate mice with a conditional *BHD* allele and introduced the cadherin 16 (KSP)–Cre transgene to target *BHD* inactivation to the kidney. Kidney cell proliferation was measured by BrdU incorporation and phospho-histone H3 staining. Kidney weight data were analyzed with Wilcoxon's rank-sum, Student's *t*, and Welch's *t* tests. Hematoxylin and eosin staining and immunoblot analysis and immunohistochemistry of cell cycle and signaling proteins were performed on mouse kidney cells and tissues. *BHD* knockout mice and kidney cells isolated from *BHD* knockout and control mice were treated with the mTOR inhibitor rapamycin. Mouse survival was evaluated by Kaplan-Meier analyses. All statistical tests were two-sided.

Results *BHD* knockout mice developed enlarged polycystic kidneys and died from renal failure by 3 weeks of age. Targeted *BHD* knockout led to the activation of Raf-extracellular signal-regulated protein kinase (Erk)1/2 and Akt-mTOR pathways in the kidneys and increased expression of cell cycle proteins and cell proliferation. Rapamycin-treated *BHD* knockout mice had smaller kidneys than buffer-treated *BHD* knockout mice had (n = 4–6 mice per group, relative kidney/body weight ratios, mean = 4.64% vs 12.2%, difference = 7.6%, 95% confidence interval = 5.2% to 10.0%; $P < .001$) and longer median survival time (n = 4–5 mice per group, 41.5 vs 23 days; $P = .0065$).

Conclusions Homozygous loss of *BHD* may initiate renal tumorigenesis in the mouse. The conditional *BHD* knockout mouse may be a useful research model for dissecting multistep kidney carcinogenesis, and rapamycin may be considered as a potential treatment for Birt-Hogg-Dubé syndrome.

J Natl Cancer Inst 2008;100:140–154

Birt-Hogg-Dubé (BHD) syndrome is an inherited kidney cancer syndrome that is characterized by benign hair follicle tumors, lung cysts, spontaneous pneumothorax, and an increased risk of renal neoplasia (1–3). We previously identified germline mutations in the *BHD* gene, which is located at chromosome 17p11.2, in BHD patients (4). Nearly all *BHD* mutations are frameshift or nonsense mutations that are predicted to prematurely truncate the BHD protein, folliculin (FLCN) (4–7). BHD patients most frequently develop bilateral multifocal chromophobe renal tumors and renal oncocytic hybrid tumors with features of chromophobe renal carcinoma and renal oncocytoma (8–10). Somatic mutations in the remaining wild-type copy of *BHD* and loss of heterozygosity at chromosome 17p11.2 have been identified in

Affiliations of authors: Urologic Oncology Branch (MB, SBH, MBW, BZ, WML, LSS) and Mouse Cancer Genetics Program (LT), Center for Cancer Research, Pathology/Histotechnology Laboratory (DCH), Basic Research Program (ES, LSS), and Small Animal Imaging Program, Laboratory Animal Sciences Program (LI), SAIC-Frederick, Inc, and Data Management Services, Inc (WGA, RL), National Cancer Institute-Frederick, Frederick, MD; Urologic Oncology Branch (MB, SBH, MBW, BZ, WML, LSS) and Molecular Imaging Program (MB, PC), Center for Cancer Research, National Cancer Institute, National Institutes of Health, Bethesda, MD; Department of Pathology, Kochi Medical School, Kochi, Japan (MF);Department of Internal Medicine, University of Texas Southwestern Medical Center, Dallas, TX (VP, PI); Department of Urology and Molecular Genetics, Yokohama City University Graduate School of Medicine, Yokohama, Japan (MY).

Correspondence to: Laura S. Schmidt, PhD, Urologic Oncology Branch, National Cancer Institute-Frederick, Bldg 560, Rm 12-69, Frederick, MD 21702 (e-mail: schmidtl@ncifcrf.gov).

See "Funding" and "Notes" following "References."

DOI: 10.1093/jnci/djm288

BHD-associated renal tumors, supporting the Knudson "two-hit" hypothesis and a tumor suppressor role for *BHD* (11).

FLCN is a 64-kDa protein with no known functional domains (4). We recently identified the FLCN-interacting protein FNIP1, which also interacts with 5′-AMP–activated protein kinase [AMPK (12)], an important energy sensor in cells that negatively regulates the mammalian target of rapamycin (mTOR), the master switch for cell growth and proliferation (13). We also demonstrated that FLCN and FNIP1 are substrates for AMPK in vitro and in vivo and that inhibition of AMPK activity reduces the phosphorylation and expression of these proteins. Phospho-FLCN levels were also reduced by inhibition of mTOR activity. Under serum-starved conditions, the level of mTOR signaling was higher in *BHD*-null renal tumor cells than in *BHD*-restored cells (12). These results suggest that FLCN may play a role in cellular energy and nutrient sensing through interactions with the AMPK-mTOR signaling pathway. Mutations in several other tumor suppressor genes, including *LKB1* (14), *PTEN* (15), and *TSC1/2* (16), have been shown to lead to dysregulation of mTOR signaling and to the development of other hamartoma syndromes. Intriguingly, recent studies in yeast have suggested that Bhd activates Tor2, in opposition to the role of Tsc1/2, which inhibits Tor2 in this model organism (17).

Animal models of human cancer provide valuable research tools for dissecting the biochemical pathways responsible for neoplasia and for testing new therapeutic agents. Renal cystadenocarcinoma nodular dermatofibrosis (RCND) in dogs (18,19) and renal tumors in the Nihon rat (20,21) occur in animals that inherit a germline mutation in the corresponding *BHD* homolog. However, these naturally occurring animal models may harbor additional genetic changes that could confound studies of the functional consequences of *BHD* inactivation. A genetically engineered mouse model provides a "clean" system with which to pursue functional studies of FLCN.

Here, we report the generation of a conditionally targeted *BHD* allele and kidney-directed *BHD* inactivation in the mouse using the KSP-Cre transgene, which contains the promoter of the kidney-specific cadherin (KSP-cadherin, cadherin 16) gene fused to Cre recombinase (22). We compared *BHD* knockout and control kidneys by histology, cell proliferation measurements, and immunostaining to evaluate the activation of Raf-Erk1/2 and Akt-mTOR pathways. We also evaluated the therapeutic effects of treatment with rapamycin, an inhibitor of mTOR, on the kidney phenotype of *BHD* knockout mice.

CONTEXT AND CAVEATS

Prior knowledge

Patients with Birt-Hogg-Dubé (BHD) syndrome who carry inactivating mutations in both copies of the *BHD* tumor suppressor gene have an increased risk for kidney cancer. Folliculin, the protein encoded by the *BHD* gene, may interact with the 5′AMP-activated protein kinase-mammalian target of rapamycin (AMPK-mTOR) signaling pathway, a key regulator of cell growth and proliferation.

Study design

Kidney-targeted *BHD* knockout mouse model to examine how loss of *BHD* affects kidney function, the potential pathways involved, and therapies that target those pathways.

Contribution

BHD knockout mice died from renal failure and had enlarged cystic kidneys due to hyperproliferation and activation of the Erk1/2 and mTOR pathways. Treatment with the mTOR inhibitor rapamycin reduced kidney size and prolonged survival.

Implications

Loss of both copies of the *BHD* gene may lead to renal tumorigenesis in the mouse. The model used in this study may also be useful to determine the mechanisms of kidney carcinogenesis.

Limitations

The mouse model used in this study may not precisely recapitulate BHD syndrome in humans; additional genetic changes may be required for progression to kidney carcinogenesis.

Materials and Methods

Generating a *BHD* Conditional Targeting Vector and Kidney-Specific *BHD*-Targeted Mouse

The *BHD* targeting vector was generated by the recombineering method, which uses homologous recombination in *Escherichia coli* strain DY380 (23). A neomycin resistance (Neo^r) cassette, flanked by *Frt* and *loxP* sequences, was inserted into intron 6 of *BHD* for positive selection, and the thymidine kinase gene was included for negative selection. A second *loxP* sequence was inserted into intron 7. The targeting vector was electroporated into mouse embryonic stem cells, which were selected for G418 resistance and gancyclovir sensitivity. Correctly targeted embryonic stem cells were identified by Southern blot analysis and injected into mouse blastocysts to produce chimeras. Backcrossing to C57BL/6 mice produced heterozygous F1 offspring with germline transmission of the *BHD floxed (f)* allele. The retained Neo cassette flanked by *Frt* sites was excised in vivo by crossing the heterozygous *BHD floxed* ($BHD^{f/+}$) F1 mice with mice expressing the Flp recombinase transgene under the ubiquitous β-actin promoter to produce $BHD^{f/+}$*/Flp* mice. Subsequently, the *Flp* transgene was removed from the $BHD^{f/+}$*/Flp* mice by backcrossing to C57BL/6 mice to produce $BHD^{f/+}$ mice. $BHD^{f/f}$ mice were generated by intercrossing $BHD^{f/+}$ mice. To produce the *BHD deleted (d)* allele, $BHD^{f/+}$ mice were crossed with mice expressing the Cre recombinase transgene under the β-actin promoter, resulting in $BHD^{d/+}$*/β-actin Cre* mice (24). The β-actin Cre transgene was removed from the $BHD^{d/+}$*/β-actin Cre* mice by backcrossing to C57BL/6 mice, resulting in $BHD^{d/+}$ mice. Deletion of exon 7 in the $BHD^{d/+}$ mice resulted in a frameshift and premature termination codon in exon 8. *KSP-Cre* transgenic mice (n = 4), which expressed Cre recombinase under the cadherin 16 promoter specifically in the adult renal tubules and developing genitourinary tract (22), were crossed with $BHD^{d/+}$ mice (n = 6) to generate $BHD^{d/+}$*/KSP-Cre* mice (n = 39). To produce mice with kidney-specific inactivation of *BHD*, $BHD^{d/+}$*/KSP-Cre* male mice (n = 10) were mated with $BHD^{f/f}$ female mice (n = 13). Littermates with the $BHD^{f/d}$*/KSP-Cre* genotype (n = 89) and $BHD^{f/+}$*/KSP-Cre* genotype (n = 84) were killed by CO_2 asphyxiation or decapitation and analyzed for phenotype at day (P) 2, P7, P14, and P21.

To verify that *BHD* knockout was targeted to the kidney and to visualize Cre expression, we developed $BHD^{f/d}$*/Rosa26lacZ/KSP-Cre*

mice. *BHD*$^{f/f}$ mice were crossed with *Rosa26lacZ* mice (obtained from Philippe Soriano, Fred Hutchinson Cancer Research Center, Seattle) to produce *BHD*$^{f/+}$*/Rosa26lacZ* mice (n = 10). *BHD*$^{f/+}$*/Rosa26lacZ* mice (n = 6) were intercrossed to produce *BHD*$^{f/f}$*/Rosa26lacZ* mice (n = 5). *BHD*$^{f/f}$*/Rosa26lacZ* female mice (n = 2) were crossed with *BHD*$^{d/+}$*/KSP-Cre* male mice (n = 2) to generate *BHD*$^{f/d}$*/Rosa26lacZ/KSP-Cre* mice.

A total of 837 mice were used in these experiments, all of which were housed in the National Cancer Institute (NCI)-Frederick animal facility in standard cages with food and water ad libitum, grouped by age, sex, and strain, according to the NCI-Frederick Animal Care and Use Committee guidelines. C57BL/6 mice were purchased from Charles River Laboratories (Frederick, MD). All other mouse strains were produced in house. Animal care procedures followed the NCI-Frederick Animal Care and Use Committee guidelines.

Southern Blot Analysis of Embryonic Stem Cells and Polymerase Chain Reaction Genotyping of *BHD* Knockout Mice

KOD Hot DNA polymerase (Novagen, Madison, WI) was used for generating probes and routine polymerase chain reaction (PCR) genotyping. A 5′ external probe for Southern blot analysis of targeted embryonic stem cells was generated by PCR with primers: forward, 5′-TCGACCTCGATGGAGTGATCC-3′; reverse, 5′-GGCAATGGCACCCATTTAAGG-3′ (GenBank NT_096135.5). A 3′ external probe was also generated by PCR with primers: forward, 5′-CAGGCTCAAGCAGTAGTGAGACCA-3′; reverse, 5′-CATTCTGCTTTGGGGCATGA-3′ (GenBank NT_096135.5). Genomic DNA was isolated from tail samples of mice using DirectPCR Reagent (Viagen Biotech, Inc., Los Angeles, CA) according to manufacturer's protocols. Nonradioactive Southern blotting was performed with DIG OMNI System for PCR probes (Roche Molecular Biochemicals, Indianapolis, IN) according to the manufacturer's protocol. PCR genotyping was performed with three primer sets to amplify wild-type (178-bp PCR product; GenBank AL596204), *floxed* (292-bp PCR product), and *deleted* (392-bp PCR product) *BHD* alleles: P1, 5′-GTTGTCTGGAGTGCTACTTAGT CAGG-3′, which is complementary to the genomic sequence upstream of the 5′-*loxP* sequence; P2, 5′-CAACACCCCAGCATCCAG-3′, which is complementary to the sequence downstream of 5′-*loxP*; and P3, 5′-CAGCTCCCTCTACCCAGACA-3′, which is complementary to the sequence downstream of 3′-*loxP*. For Cre genotyping, the forward (5′-GCAACATTTGGGCCAGCTAAAC-3′) and reverse (5′-CCGGCATCAACGTTTTCTTTTC-3′) primers (GenBank AB363405) were used for PCR amplification.

Antibodies

The following antibodies were used: horseradish peroxidase–labeled goat anti-mouse IgG, goat anti-rabbit IgG, rabbit polyclonal cyclin A, rabbit monoclonal cdc2, and rabbit polyclonal vacuolar-H^+ATPase (Santa Cruz Biotechnology, Santa Cruz, CA); acetylated tubulin (Sigma, St Louis, MO); rabbit polyclonal Na-K-Cl cotransporter 2 (NKCC2) (Chemicon, Temecula, CA); rabbit polyclonal thiazide-sensitive Na-Cl cotransporter (TSC, gift from Mark Knepper); lectin *Dolichos biflorus* agglutinin (DBA) and lectin *Lotus tetragonolobus* agglutinin (LTA) (Vector Laboratories, Burlingame, CA); rabbit monoclonal phospho-S6 ribosomal protein (S6R), rabbit monoclonal S6R, rabbit polyclonal phospho-AKT, rabbit polyclonal AKT, rabbit monoclonal phospho-AMPKα, rabbit polyclonal AMPKα1, rabbit monoclonal cyclin D1, rabbit monoclonal phospho-c-Raf, rabbit polyclonal phospho-MEK1/2, rabbit polyclonal phospho-Erk1/2, rabbit polyclonal phospho-p90RSK, rabbit polyclonal phospho-mTOR, and rabbit polyclonal mTOR (Cell Signaling, Danvers, MA); rabbit polyclonal actin (Biomedical Technology, Stoughton, MA); mouse monoclonal BrdU (DAKO, Carpinteria, CA); rabbit polyclonal phospho-histoneH3 (Upstate, Charlottesville, VA); rabbit polyclonal cdk4 (Clontech, Mountain View, CA); and rabbit polyclonal cyclin B1 [(25) gift from Philipp Kaldis]. FLCN-105, a rabbit polyclonal antibody against GST-FLCN, and FLCN-mAb in culture medium from single clone hybridoma cell line raised against full-length GST-FLCN in the mouse were prepared as described previously (12).

Immunoblot Analysis of Folliculin and Quantitative Reverse Transcription-Polymerase Chain Reaction Expression Analysis of the *BHD* Gene

Three-week-old mice were killed by CO_2 asphyxiation (n = 3 each genotype), and their kidneys were removed, cut into small pieces, snap frozen in liquid nitrogen, and stored at –80°C until further analysis. For each mouse, one frozen kidney piece was homogenized in radioimmunoprecipitation assay buffer (20 mM Tris-HCl, pH 7.5, 150 mM NaCl, 1 mM EDTA, 1 mM Na_3VO_4, 50 mM NaF, 1.0% Triton X-100, 0.5% deoxycholate, 0.1% sodium dodecylsulfate [SDS], 100 nM calyculin A, and Complete Protease Inhibitor cocktail [Roche, Molecular Biochemicals, Indianapolis, IN]) with a Polytron homogenizer on ice followed by centrifugation at 16000 × g for 30 minutes. Protein concentrations of cleared supernatants were measured with the BCA Protein Assay Kit (Pierce, IL) and adjusted to 1.33 mg/mL, 4× SDS-sample buffer was added, and samples were boiled for 5 minutes to produce 1 mg/mL sample lysates. A total of 20 μg of protein was subjected to 4%–20% or 4%–15% SDS-polyacrylamide gel electrophoresis. Immunoblotting was performed as previously described (12). Antibodies were diluted as follows: mouse monoclonal FLCN, 1:1000; β- actin, 1:500; cyclin D1, 1:1000; cyclin A, 1:1000; cyclin B1, 1:1000; cdc2, 1:1000; CDK4, 1:1000; phospho-c-Raf(Ser338), 1:1000; phospho-MEK1/2(Ser217/221), 1:1000; phospho-Erk1/2(Thr201/Tyr204), 1:1000; phospho-p90RSK(Ser380), 1:1000; phospho-Akt(Thr308), 1:1000; Akt, 1:1000; phospho-mTOR(Ser2448), 1:1000; mTOR, 1:1000; phospho-S6R(Ser240/244), 1:1000; S6R, 1:1000; phospho-AMPKα, 1:500. At least three independent experiments were performed with two replicates each. Secondary antibodies were diluted as follows: goat anti-mouse IgG–horseradish peroxidase, 1:1000; goat anti-rabbit IgG–horseradish peroxidase, 1:1000 (Santa Cruz Biotechnology, SantaCruz, CA). Antibody–protein complexes were detected using ECL Western Blotting Detection Reagent (Amersham, Buckinghamshire, UK) according to the manufacturer's instructions.

Total RNA was isolated from frozen kidney tissues (one sample per kidney, one kidney sample per mouse) using Trizol reagent (Invitrogen, Carlsbad, CA) according to the manufacturer's instructions. Quantitative reverse transcription (qRT)-PCR was performed as previously described (26). The following PCR primers to amplify β-actin and *BHD* exons 6 and 7 were generated by

using Primer 3 software: β-actin forward: 5′-GACAGGATGCAG AAGGAGATTACTG-3′, β-actin reverse: 5′-GCTGAT CCACATCTGCTGGAA-3′ (GenBank NM_007393.3); *BHD* forward: 5′-GATGACAACTTGTGGGCGTGTC-3′, *BHD* reverse: 5′-CATCTGGACCAGGGTGTCCTCT-3′ (GenBank NM 146018.1). Three independent experiments were performed in triplicate using the β-actin gene as an internal control.

Magnetic Resonance Imaging to Examine Kidney Function in *BHD$^{f/d}$/KSP-Cre* Mice

Three-week-old *BHD$^{f/+}$/KSP-Cre* and *BHD$^{f/d}$/KSP-Cre* mice (n = 2 for each genotype) were kept under isoflurane gas anesthesia (1%–2% isoflurane in O_2) at approximately 80 breaths per minute in a cylindrical chamber and imaged in a clinical 3.0 T magnetic resonance imaging (MRI) scanner (Philips Intera Achieva, Best, The Netherlands) using a 40-mm diameter solenoid volume receiver coil (Philips Research, Hamburg, Germany). Multislice T_2-weighted fast spin echo (T2W-FSE) images (timed repetition [TR] = 2823 ms, echo time [TE] = 65 ms, flip angle [FA] = 90, matrix 352 × 170, field of view [FOV] = 60 × 30 mm, slices = 32, thickness = 0.5 mm, scan time = 6:26 minutes) were acquired in the coronal plane with respiratory triggering to minimize motion artifacts. Dynamic contrast-enhanced MRI was performed by taking a series of T_1W-SPGR images (TR = 20 ms, TE = 3 ms, FA = 24, matrix = 512 × 130, FOV = 60 × 30 mm, slices = 32, thickness = 0.5 mm, scan time = 2:43 minutes) in the coronal plane every 3 minutes for 30 minutes. After the first dynamic image, 50 μL of an 80 mM dilution of gadolinium (Gd) contrast agent (Magnevist, Bayer HealthCare Pharmaceuticals, Wayne, NJ) in phosphate-buffered saline (PBS; 137 mM NaCl, 10 mM phosphate, 2.7 mM KCl, pH 7.4; nominal dosage of 0.2 mmol Gd/kg mouse) along with an additional 50 μL of PBS was infused at a rate of 150 μL per minute into the tail vein through a catheter using a syringe pump (BS-9000-8, Braintree Scientific, Braintree, MA). Dynamic subtraction images were obtained by subtracting the precontrast image from each of the postcontrast images.

Phenotype Evaluation and Histopathology

BHD$^{f/d}$/KSP-Cre mice (n = 60) and control *BHD$^{f/+}$/KSP-Cre* mice (n = 70) were weighed, killed by CO_2 asphyxiation (for P14 and P21) or decapitation (for P0, P1, and P7), and dissected. Kidneys were removed, weighed, fixed in 10% neutral-buffered formalin for 24 hours, and subjected to fixation in 70% ethanol. Kidneys were then routinely processed, embedded in paraffin, sectioned at 5 μm and stained with hematoxylin and eosin (H&E). Stained sections were evaluated by a board-certified veterinary pathologist (D. C. Haines). To measure dried weight, dissected kidneys from *BHD$^{f/+}$/KSP-Cre* mice (n = 8) and *BHD$^{f/d}$/KSP-Cre* mice (n = 6) were minced into small pieces and dried by vacuum centrifugation at 50°C overnight.

Blood Urea Nitrogen Analyses to Measure Kidney Function

Blood was collected into a Microvette CB300 (Sarstedt, Germany) from decapitated P0, P2, and P7 *BHD$^{f/+}$/KSP-Cre* and *BHD$^{f/d}$/KSP-Cre* mice. P14 and P21 mice were killed by CO_2 asphyxiation, and a cut was made in the right atrium. Blood was collected by pipet, transferred into a Microvette CB300, and centrifuged at 10 000 × *g* for 5 minutes at 20°C. Serum was collected and stored at −80°C for further analysis. Serum samples were placed on a Vitros blood urea nitrogen (BUN)/urea slide, and BUN measurements were performed on a Vitros 250 instrument according to the manufacturer's protocol (Ortho-Clinical Diagnostics, Rochester, NY).

Rapamycin Treatment of *BHD$^{f/d}$/KSP-Cre* and Control *BHD$^{f/+}$/KSP-Cre* Mice

BHD$^{f/d}$/KSP-Cre and control *BHD$^{f/+}$/KSP-Cre* mice at P7 were randomly divided into two groups for buffer (n = 11) and rapamycin (n = 10) treatment. Rapamycin (LC Laboratories, MA) was dissolved in 100% ethanol at a stock concentration of 10 mg/mL. Rapamycin stock solution was diluted to 200 μg/mL in buffer (5% Tween 80, 5% PEG400) and injected intraperitoneally at a dose of 2 mg/kg daily. At day 21 or before, if moribund (usually day 19 or 20), mice were killed, kidneys were dissected, kidney/body weight ratios were measured, and histopathology was performed as described above.

For survival analysis, *BHD$^{f/d}$/KSP-Cre* mice at P7 were randomly divided into two groups for buffer (n = 5) and rapamycin (n = 4) treatment. Rapamycin (2 mg/kg per day) or buffer was injected daily intraperitoneally until mice were found dead or moribund.

Renal Tubule Cell Primary Culture

One *BHD$^{f/+}$/KSP-Cre* and one *BHD$^{f/d}$/KSP-Cre* mouse were euthanized at P21 and perfused with Liver Perfusion Medium (Invitrogen) and Liver Digest Medium (Invitrogen). After perfusion, kidneys were removed using aseptic technique, minced into small pieces with a razor blade, and incubated in Liver Digest Medium on a rocker at 37°C for 20–45 minutes. Digested tissues were dissociated by gentle pipetting, washed with Hepatocyte Wash Medium (Invitrogen), and incubated with Accutase (Innovative Cell Technologies, Inc., San Diego, CA) on a rocker at 37°C for 15 minutes. Dissociated tissues were filtered through a 40-μm cell strainer (BD Biosciences, San Jose, CA) twice, washed with Hepatocyte Wash Medium, resuspended in PBS/0.02% EDTA, and separated by Percoll gradient centrifugation to isolate the tubule cell fraction that fractionated between the PBS and 41.9% Percoll/1X MEM layers. Isolated tubule cell fractions were washed three times with SFFD Medium (Dulbecco's Modified Eagle's Medium, Ham's F-12 [1:1], 10 mM Hepes, 1.1 mg/mL sodium bicarbonate, 10 nM sodium selenium) and plated on collagen-I-coated dishes (BD Biosciences) in 10% fetal bovine serum/SFFD medium. After 24 hours, dishes were washed twice with PBS, and medium was replaced with K1 Medium (SFFD medium with 5 μg/mL insulin, 25 ng/mL PGE1, 5 pM triiodothyronine [T3], 50 nM hydrocortisone, and 5 μg/mL apo-transferrin). Cells were detached from culture dishes by washing with PBS/0.02% EDTA followed by incubation at 37°C for 15 minutes with Accutase. For cell growth assays, 1×10^4 cells were plated on 3.5-cm collagen-I-coated dishes with K1 medium containing 10 nM rapamycin or DMSO diluent as control. Cells were detached from three dishes for each group at each time point by incubation with Accutase and counted using a hemocytometer with two replicates.

Immunohistochemistry and Immunofluorescence Analysis of Cell Cycle Markers and Akt-mTOR and Erk-MEK 1/2 Pathway Signaling

Sections (5 μm) from formalin-fixed, paraffin-embedded tissues were placed on slides for immunohistochemistry. Phospho-histone

H3 staining was performed using the Ventana automated immunohistochemistry system (Ventana HX system Dyscovery/20: 750-DSC, Ventana Medical systems, Inc., Tucson, AZ). Antigen retrieval was performed by microwave-heated incubation in citrate buffer for 20 minutes, followed by incubation with rabbit polyclonal anti–phospho-histone H3 (1:5000) overnight at 4°C. For immunofluorescence staining, the renal capsules were removed from the kidneys of P0, P2, and P7 mice (n = 3 at each age) in ice-cold PBS, and kidneys were fixed in 4% paraformaldehyde (PFA) for 1.5 hours at 4°C, followed by sucrose replacement (5%–20% sucrose/0.1M sodium phosphate, pH 7.2). Kidneys were then embedded in Optimal Cutting Temperature (OCT) compound, frozen on a metal block in liquid nitrogen, and stored at −80°C. P14 and P21 mice (n = 3 at each age) were killed and perfusion fixed with 4% PFA. Kidneys were removed, further fixed in 4% PFA for 1 hour at 4°C, subjected to sucrose replacement, embedded in OCT compound, and frozen as above. Frozen sections (5 μm) were prepared (n = 20 per mouse), mounted on slides, fixed in methanol/acetone (1:1) at −20°C for 10 minutes, and blocked with 10% normal goat serum. The slides were then rinsed with PBS, quenched in 0.5 M ammonium chloride/0.1% bovine serum albumin (BSA) in PBS for 15 minutes at room temperature, washed with PBS, and incubated with the primary antibody in buffer containing 10 mM Tris-HCl, pH 7.5, 150 mM NaCl, 0.01% (v/v) Tween 20, 3% goat serum, and 0.1% (w/v) BSA at 4°C overnight. Antibodies and dilutions were as follows: DBA, 1:400; NKCC2, 1:1000; LTA, 1:400; TSC, 1:400; vacuolar H^+-ATPase, 1:200; cyclin D1, 1:50; P-Erk1/2, 1:100; P-Akt, 1:100; P-mTOR, 1:100; P-S6R, 1:100. After three 10-minute washes with Tris-buffered saline/Tween 20 (TBST) (10 mM Tris-HCl, pH 7.5, 150 mM NaCl, 0.01% [v/v] Tween 20), slides were incubated with Alexa Fluor 488 goat anti-rabbit IgG (1:500 dilution) and/or Alexa Fluor 594 goat anti-mouse IgG (1:500 dilution) (Invitrogen). After another three 10-minute washes with TBST, slides were sealed with mounting medium containing 4′-6-Diamidino-2-phenylindole (Vector Laboratories) and viewed with a confocal microscope system (LSM 510; Carl Zeiss, Thornwood, NY).

Kidney tumor tissue (n = 16; 10 tumors from patient 1, three tumors from patient 2, two tumors from patient 3, and one tumor from patient 4) and normal kidney parenchyma (n = 4; two normal tissues from patient 2 and one each normal tissues from patients 3 and 4) samples from BHD patients who had been surgically treated at the Urologic Oncology Branch, National Institutes of Health (NIH), Bethesda, MD (with patient permission under an NIH Institutional Review Board–approved protocol #97-C-0147) were frozen in OCT compound without fixation. Frozen sections were fixed in methanol/acetone (1:1) at −20°C for 10 minutes followed by staining with phospho-mTOR antibody using the procedure above.

For cell proliferation measurements, BrdU (100 μg/g body weight) was injected intraperitoneally into P14 $BHD^{f/+}$/*KSP-Cre* (n = 2) and $BHD^{f/d}$/*KSP-Cre* (n = 2) mice, and, 2 hours later, the mice were killed by CO_2 asphyxiation. Kidneys were fixed with 10% formalin for 24 hours, followed by fixation in 70% ethanol. Sections that were 5 μm in thickness (n = 4) were immunostained with mouse monoclonal anti-BrdU antibody (1:500) after trypsin pretreatment for 3 hours at 37°C using the ARK kit (DAKO). The number of BrdU-stained cells per 1000 cells in each field was counted in five randomly selected fields. β-galactosidase activity was measured in situ in frozen sections (n = 2 per mouse) prepared as described above using standard staining techniques. Tissue sections were counterstained with nuclear fast red (Sigma).

Statistical Analysis

Data were analyzed using both parametric and nonparametric methods and graphical techniques. Kidney weight data were analyzed with Wilcoxon's rank-sum test, Student's *t* test, and Welch's *t* test to account for unequal within-group variances. Cell count and longitudinal growth data were analyzed with regression analysis, analysis of variance, and analysis of covariance following logarithmic (base 10) transformation of the data to satisfy the homogeneity of variance assumptions underlying the models. Where appropriate, results are reported or plotted with 95% confidence intervals (CIs). Mouse survival time was defined as the time from birth until the animals died or became moribund. Survival data were estimated and plotted with the Kaplan-Meier method; differences between survival groups were assessed with the log-rank test. Statistical analyses were performed with S-Plus (version 7.0, Insightful Corporation, Seattle, WA) and SAS (version 9.1, Cary, NC). All statistical tests were two-sided. *P* values less than .05 were considered to be statistically significant.

Results

We determined that homozygous *BHD* deletion is embryonic lethal in the mouse because no $BHD^{d/d}$ offspring were produced from intercrosses of $BHD^{d/+}$ mice (data not shown). To circumvent embryonic lethality, we developed a conditional *BHD* knockout mouse. The targeting vector, with *loxP* sites flanking exon 7 of the *BHD* gene, was generated by recombineering methodology (27) (Fig. 1, A). Correctly targeted embryonic stem cell clones were selected by Southern blot screening (Fig. 1, B) and used to generate chimeric mice that were then backcrossed to C57BL/6 mice for germline transmission of the *BHD floxed (f)* allele.

To target *BHD* deletion to the kidney specifically, we used *Cre* transgenic mice expressing Cre recombinase under the KSP-cadherin (cadherin 16) promoter, which drives Cre expression exclusively in kidney tubule epithelial cells and in the developing genitourinary tract (22). $BHD^{d/+}$/*KSP-Cre* mice were generated by crossing $BHD^{d/+}$ mice with *KSP-Cre* mice. Conditionally deleted $BHD^{f/d}$/*KSP-Cre* mice and $BHD^{f/+}$/*KSP-Cre* littermate controls were produced from $BHD^{f/f}$ and $BHD^{d/+}$/*KSP-Cre* parents. Mice with kidney-specific inactivation of *BHD* appeared normal at birth but showed distended abdomens by 2 weeks, which were very pronounced at the time of death, at approximately 3 weeks of age. At autopsy, the enlarged kidneys completely filled the abdominal cavity, and this phenotype was 100% penetrant in $BHD^{f/d}$/*KSP-Cre* mice (Fig. 2, A). MRI with gadolinium enhancement revealed highly cystic features and a fine reticular pattern of interstitial tissue containing numerous blood vessels in the *BHD*-inactivated kidneys (Fig. 2, B), which were not seen in control kidneys (data not shown). BHD mRNA expression levels (relative to internal β-actin controls as measured by qRT-PCR) in *BHD*-inactivated kidneys (Fig. 2, D) were statistically significantly lower than those of control kidneys ($BHD^{f/+}$/*KSP-Cre* to $BHD^{f/d}$/*KSP-Cre*, expression normalized to control value: mean = 1.09 vs 0.11,

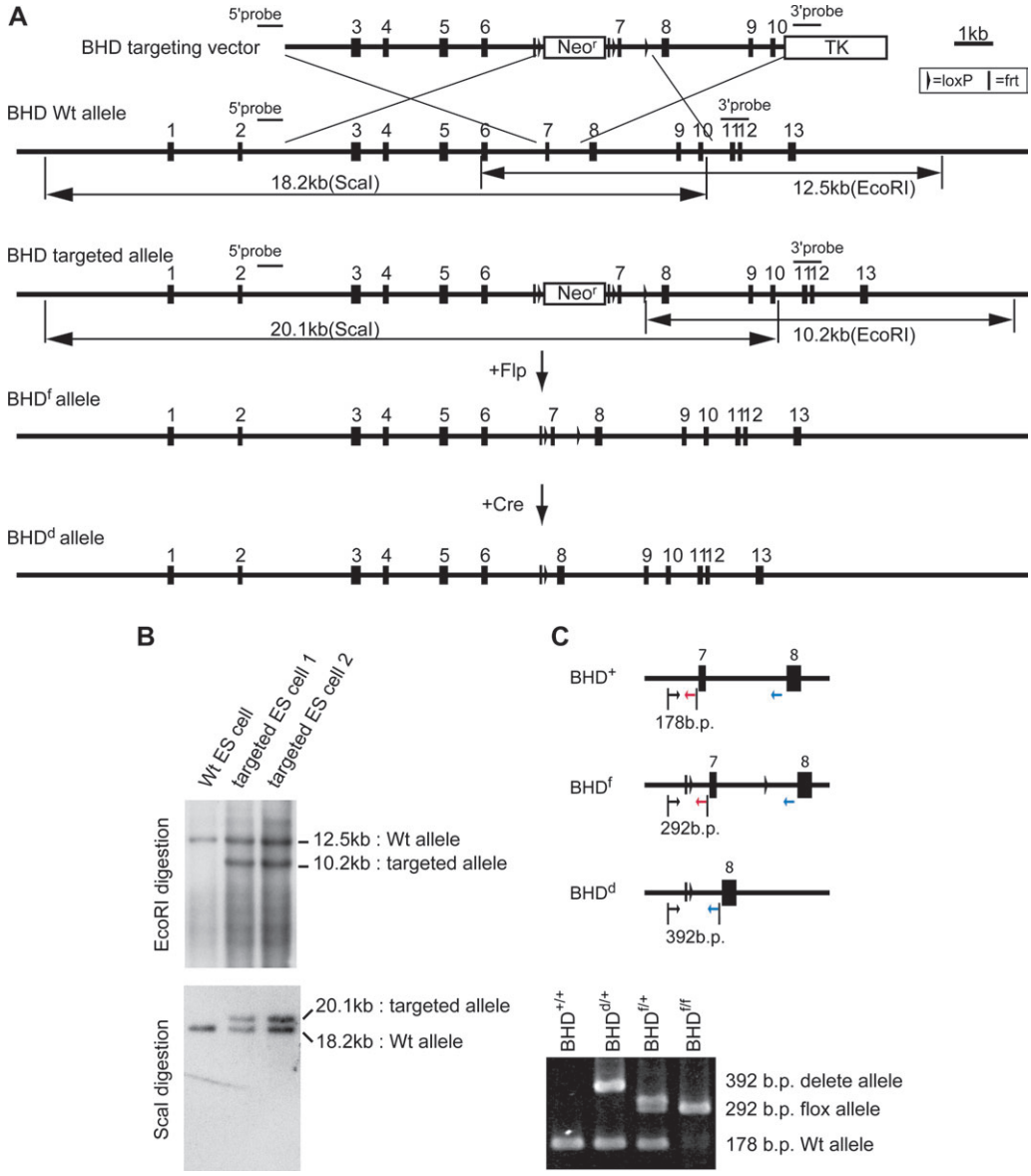

Fig. 1. Generation of conditional Birt-Hogg-Dubé (*BHD*) knockout mice. **A**) Targeting strategy. *BHD* gene–targeting vector was constructed by recombineering methodology using homologous recombination (27). A neomycin resistance (Neo^r) cassette flanked by *Frt* (**bar**) and *loxP* (**triangle**) sequences was inserted into intron 6 for positive selection, and the thymidine kinase gene was included for negative selection. A second *loxP* sequence was inserted into intron 7. Correctly targeted embryonic stem cells were identified by Southern blot analysis and injected into blastocysts to produce chimeras. Backcrossing to C57BL/6 mice produced heterozygous F1 offspring with germline transmission of the *BHD floxed (f)-Neo* allele. The Neo cassette flanked by *Frt* sites was excised in vivo by crossing with mice expressing the Flp recombinase transgene under the β-actin promoter. To produce the *BHD deleted (d)* allele, *BHD*$^{f/+}$ mice were crossed with mice expressing the Cre recombinase transgene under the ubiquitous β-actin promoter (24). Deletion of exon 7 resulted in a frameshift and premature termination codon in exon 8, which caused mRNA degradation by the nonsense-mediated decay mRNA surveillance system (28). **B**) The targeted embryonic stem cells were screened by Southern blotting of *Eco*RI- and *Sca*I-digested DNA using two different external probes located outside the targeting sequence as shown in (**A**). **C**) Polymerase chain reaction (PCR)–based genotyping was performed using DNA extracted from mouse tails for routine monitoring of inheritance in offspring. Locations of PCR primers are indicated by **arrows**.

difference = 0.98, 95% CI = 0.80 to 1.16; $P < .001$), showing efficient Cre-mediated deletion of the floxed *BHD* sequences and probable nonsense-mediated decay of the mutant BHD mRNA. In support of these results, levels of FLCN protein were lower in *BHD*-inactivated kidneys (Fig. 2, E) than in kidneys of control littermates.

Macroscopic images of H&E-stained kidneys from *BHD*$^{f/d}$/*KSP-Cre* mice and control *BHD*$^{f/+}$/*KSP-Cre* littermates revealed no differences at birth or postnatal day (P)2. By 1 week, *BHD*-inactivated kidneys began to enlarge due to dilation of collecting ducts and some cortical tubules. At 2 weeks, lumens of ducts and tubules were cystic, causing further gross enlargement of the kidneys. At 3 weeks, the kidneys were markedly cystic, the anatomic distinction between cortex and medulla was disrupted, and regions of pyramidal infarctions were observed (Fig. 2, F). We calculated the relative ratio of kidney to body weight in *BHD*-inactivated mice and control littermates. No statistically significant differences were seen at P2. However, the kidney to body weight ratio in *BHD*$^{f/d}$/*KSP-Cre* mice increased dramatically between P7 and P21 and was statistically significantly

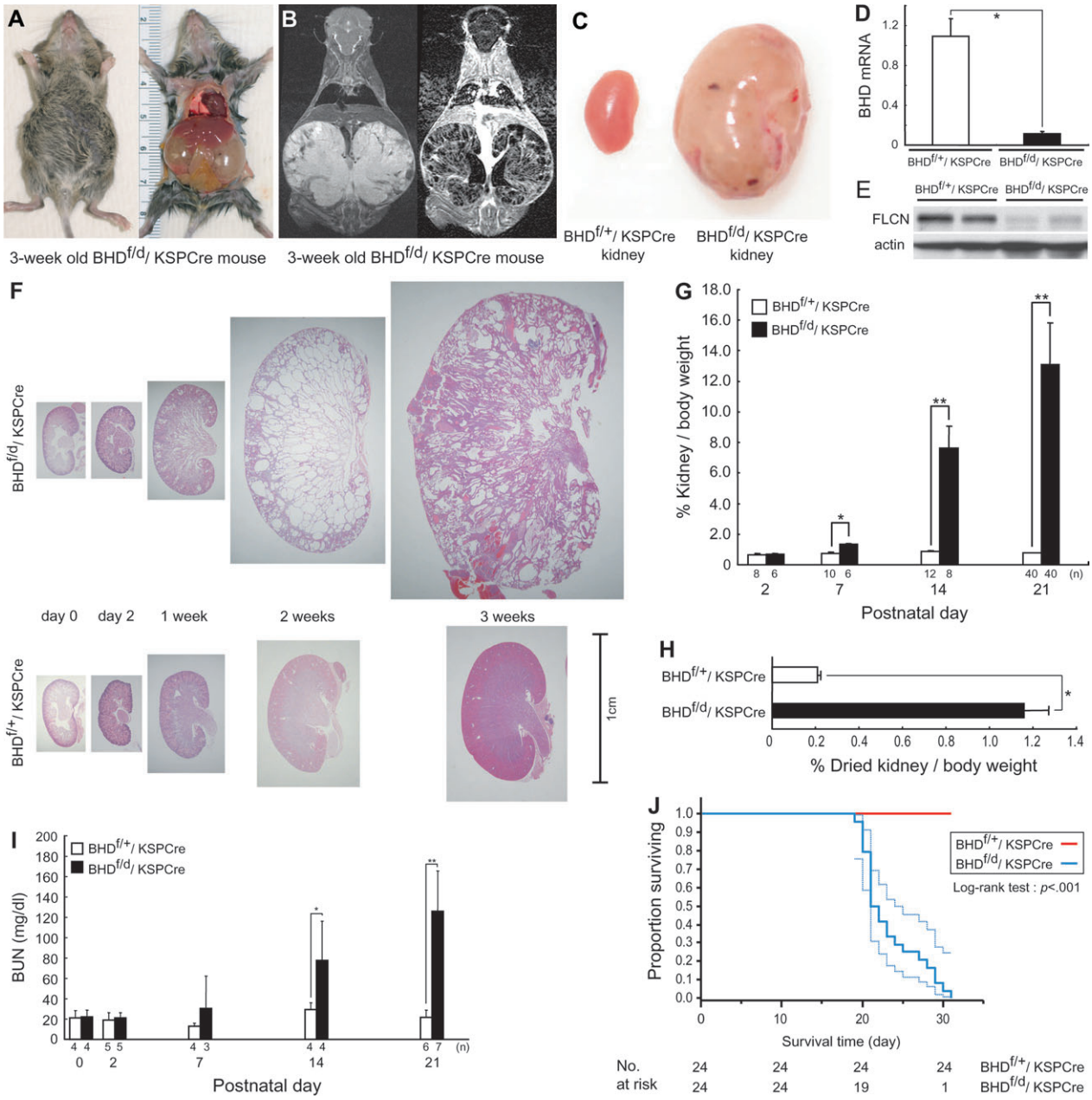

Fig. 2. Phenotypic features of Birt-Hogg-Dubé (*BHD*)–targeted deletion in the kidney. **A**) Gross picture of a 3-week old *BHD*$^{f/d}$/KSP–*Cre* mouse shows a distended abdomen (**left panel**). The large cystic kidneys fill the abdominal cavity (**right panel**) and are found in all *BHD*$^{f/d}$/*KSP-Cre* mice. **B**) T_2-weighted coronal magnetic resonance imaging (MRI) image (**left**) and corresponding gadolinium-enhanced T_1-weighted dynamic subtraction MRI image (**right**) of a 3-week-old *BHD*$^{f/d}$/*KSP-Cre* mouse show enlarged cystic kidneys with reticular interstitium and delayed excretion of contrast medium. **C**) Comparison of gross features of 3-week-old control *BHD*$^{f/+}$/*KSP-Cre* and knockout *BHD*$^{f/d}$/*KSP-Cre* kidneys reveals symmetric enlargement without focal masses in knockout *BHD*$^{f/d}$/*KSP-Cre* kidneys. One representative image of 40 mice for each genotype is shown. **D**) BHD mRNA expression in kidneys of 3-week-old mice as quantified by quantitative reverse transcription-polymerase chain reaction (qRT-PCR) using exon 6 and 7 amplification. Three mice of each genotype were analyzed. Data are presented as means and 95% confidence intervals (CIs) from three independent experiments, each performed in triplicate (Welch's *t* test, two-sided,*P < .001). **E**) Folliculin (FLCN) expression in control and knockout kidneys was estimated by immunoblot analysis. One representative of three independent experiments performed in two mice is shown. **F**) Comparison of *BHD* control and knockout kidney histology (hematoxylin and eosin staining) at different ages shows no obvious differences at days 0 and 2. At 1 week, *BHD* knockout mice have enlarged kidneys with dilated collecting ducts and a few dilated cortical tubules. By 2 weeks, most collecting ducts in the medulla are markedly dilated. The entire *BHD* knockout kidney is diffusely filled with cystic collecting ducts and tubules by 3 weeks, and the anatomic distinction between cortex and medulla is lost. One representative of at least three mice at each age is shown. **G**) Relative ratio of kidney to body weight (BW; 100% × kidney weight/[BW–kidney weight]) was calculated at different ages. Data are shown as means and 95% confidence intervals (*P = .002, **P < .001, two-sided, Welch's *t* test). **H**) Relative ratio of dried kidney to body weight (100% × dried kidney weight/[BW–wet kidney weight]) of 3-week-old mice was calculated. Data are represented as means and 95% confidence intervals (*P < .001, two-sided, Welch's *t* test). **I**) *BHD*$^{f/d}$/*KSP-Cre* mice die of renal failure. Blood urea nitrogen (BUN) levels were determined at different ages. Data are represented as means and 95% confidence intervals (*P = .03, **P = .0012, two-sided, Welch's *t* test). **J**) Kaplan-Meier survival analysis shows a statistically significant difference between control and *BHD* knockout mice for overall survival (two-sided log-rank test, P < .001). Median survival time of *BHD* knockout mice is 21.5 days (n = 24). **Dotted lines**, 95% confidence intervals.

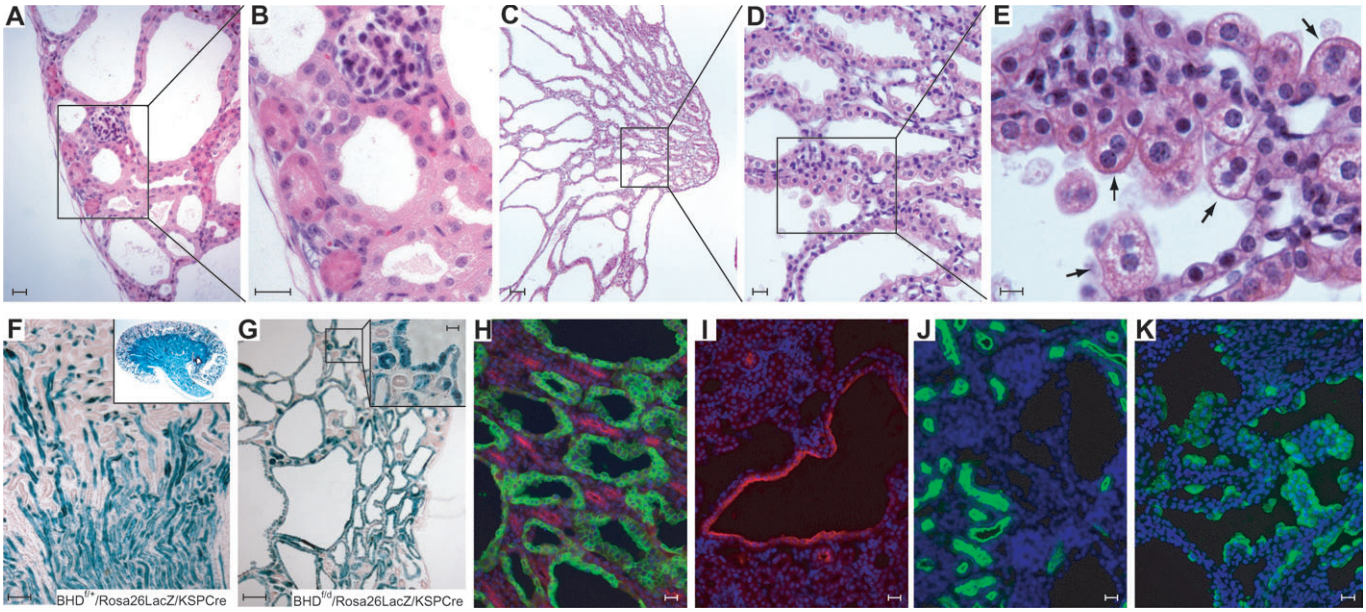

Fig. 3. Histology and immunostaining of kidneys of Birt-Hogg-Dubé (*BHD*) knockout mice. (**A**–**E**) Histology of hematoxylin and eosin–stained kidney from a 3-week-old *BHD*$^{f/d}$/*KSP-Cre* mouse. **A**) The subcapsular region of the kidney shows dilated distal tubules, mildly compressed glomeruli, and relatively normal proximal tubules. One representative image of 10 sections is shown. **B**) Higher magnification of (**A**). Bowman's space is minimal and glomerular tufts are mildly compressed. Morphologically normal proximal tubules are surrounded by dilated distal tubules lined by hypertrophic cells with enlarged eosinophilic granular cytoplasm and enlarged nuclei. **C**) Collecting ducts in the medulla are severely dilated. (**D**–**E**) Higher magnification of medulla. Hypertrophic cells with enlarged eosinophilic, granular cytoplasm that protrude into the lumen and an occasional binucleated cell are evident (**arrow**). **F**) To confirm the Cre expression pattern in the kidney, *BHD*$^{f/f}$/*Rosa26lacZ* mice were generated and crossed with *BHD*$^{d/+}$/*KSP-Cre* mice. Representative X-Gal staining of a *BHD*$^{f/+}$/*Rosa26lacZ*/*KSP-Cre* mouse kidney at 3 weeks of age shows strong staining in the medulla and scattered staining pattern in the cortex. **G**) All dilated tubules of 3-week-old *BHD*$^{f/d}$/*Rosa26lacZ*/*KSP-Cre* mouse kidneys show strong X-Gal staining. Morphologically normal proximal tubules also show mosaic staining (inset). **H**) *Dolichos biflorus* agglutinin (DBA; **green**) and Na-K-Cl cotransporter 2 (NKCC2; **red**) staining in 1-week-old *BHD*$^{f/d}$/*KSP-Cre* mouse kidneys. Dilated tubules are DBA (collecting duct marker) positive. Loops of Henle, which are NKCC2 positive, are morphologically normal. **I**) Dilated tubules in the cortex are thiazide-sensitive Na-Cl-cotransporter (TSC; **red**) positive, a marker of distal tubule. **J**) *Lotus tetragonolobus* agglutinin (LTA; **green**) staining of *BHD*$^{f/d}$/*KSP-Cre* mouse kidneys identifies apparently normal proximal tubules but does not stain dilated tubules. **K**) Markedly hypertrophic cells lining the dilated ducts of 2-week-old *BHD* knockout mouse kidneys are stained by the intercalated cell marker, vacuolar H^+-ATPase (**green**). **Scale bar** = 20 μm for A, B, D, H–K; 10 μm for E; 100 μm for C,F,G.

greater than that in littermate controls (at P21, mean ratio of kidney to body weight in *BHD*$^{f/d}$/*KSP-Cre* vs *BHD*$^{f/+}$/*KSP-Cre* mice, 13.1% vs 0.77%, difference = 12.3%, 95% CI = 11.1% to 13.6%; Fig. 2, C and G). To adjust for the weight of the fluid in the dilated tubules and ducts, kidneys from 3-week-old mice were completely dehydrated and reweighed (Fig. 2, H). The ratio of dried kidney to body weight was also greater in *BHD* knockout mice than in control littermates (*BHD*$^{f/d}$/*KSP-Cre* vs *BHD*$^{f/+}$/*KSP-Cre*: mean = 1.16% vs 0.21%, difference = 0.95%, 95% CI = 0.84% to 1.06%; $P < .001$).

To evaluate renal function in mice with *BHD*-inactivated kidneys, BUN levels were measured at different ages and compared with those of littermate controls (Fig. 2, I). BUN levels, like kidney to body weight ratios, showed no differences at birth or P2 and only slight changes at 1 week, and were statistically significantly elevated at 2 weeks ($P = .03$) and 3 weeks ($P = .0012$) in *BHD*$^{f/d}$/*KSP-Cre* mice compared with littermate controls. Renal failure in 3-week-old *BHD*$^{f/d}$/*KSP-Cre* mice may have resulted from the compression of glomeruli caused by the high density of markedly dilated tubules. The *BHD*$^{f/d}$/*KSP-Cre* mice survived for a median of 21.5 days (n = 24; Fig. 2, J); 100% of *BHD*$^{f/+}$/*KSP-Cre* littermate controls (n = 24) remained alive during this time ($P < .001$).

Histologic analysis of kidneys from 3-week-old *BHD*$^{f/d}$/*KSP-Cre* mice (Fig. 3, A–E) revealed marked enlargement due to dilated/cystic tubules and ducts extending from the renal capsule to the tip of the renal papilla, with the largest luminal diameters in the outer medulla. Most of the cells lining the dilated tubules and ducts were hypertrophic with enlarged cytoplasm and nuclei, and many cells were hyperplastic. The subcapsular region of the distorted cortex contained dilated distal convoluted tubules, which were interspersed with morphologically normal proximal tubules, and mildly compressed glomeruli (Fig. 3, A and B). In the medulla and extending into the papilla, the collecting ducts were severely cystic (Fig. 3, C and D). We noted larger hypertrophic cells, particularly in the medulla, with eosinophilic granular cytoplasm and well-defined cell borders that frequently protruded into the cystic lumen. The centrally located, round nuclei varied in size from normal, with stippled chromatin and one or more inconspicuous nucleoli, to twice normal size with more euchromatin and a more prominent single nucleolus. An occasional binucleated cell was noted (Fig. 3, E). These "oncocytic-like" cells had some of the features of cells in regions of renal "oncocytosis" found in apparently normal renal parenchyma of BHD patients (8). Thin loops of Henle were present in the medulla and showed minimal dilatation.

To determine the location of KSP-driven Cre expression, we generated *BHD*$^{f/d}$*/Rosa26lacZ/KSP-Cre* indicator offspring. KSP-driven Cre expression will delete a Neo expression cassette flanked by *loxP* sites upstream of the *lacZ* gene, thereby permitting β-galactosidase expression and its detection by 5-bromo-4-chloro-3-indolyl-D-galactoside (X-Gal) staining in tissue sections. X-Gal staining confirmed KSP-driven Cre expression in all cells lining the cystic tubules and ducts (Fig. 3, G). KSP-driven Cre expression was also detected in some proximal tubules that were morphologically normal (inset, Fig. 3, G).

To classify cystic structures, immunohistochemical analyses were performed on sections from 1-week-old *BHD*$^{f/d}$*/KSP-Cre* kidney sections using DBA [collecting duct marker (29)], NKCC2 [loop of Henle marker (30)], LTA (proximal tubule marker (31)], and thiazide-sensitive Na-Cl-cotransporter [TSC, distal tubule marker (32)] antibodies. Staining patterns in *BHD*-inactivated kidneys confirmed the histologic findings that the distal tubules and collecting ducts were dilated (Fig. 3, H and I), whereas the proximal tubules and loops of Henle were relatively normal in appearance (Fig. 3, H and J). Chromophobe renal carcinoma, oncocytoma, and oncocytic hybrid tumors are the most common renal tumors found in BHD patients, and evidence suggests that they arise from intercalated cells (33,34). Interestingly, strong immunofluorescence staining for the intercalated cell marker vacuolar-H^+-ATPase (35) was observed in 3-week-old *BHD*-inactivated kidneys in the numerous hypertrophic cells with oncocytic-like features (8) that line the dilated ducts (Fig. 3, K).

The increased size and weight of *BHD*-inactivated kidneys suggested that the cells were hyperproliferating. To evaluate cell proliferation directly, BrdU incorporation into mouse kidneys was measured by immunostaining. More kidney cells from *BHD*$^{f/d}$*/KSP-Cre* mice than *BHD*$^{f/+}$*/KSP-Cre* mice were stained with BrdU (mean = 121.8 cells per 1000 cells vs 9.6 cells per 1000 cells, difference = 112.2 cells, 95% CI = 59.3 to 165.0 cells; $P = .004$; Fig. 4, A–C). To evaluate proliferating cells in the G2/M phase of the cell cycle, phospho-histone H3 immunostaining was performed on kidney sections. More phospho-histone H3–stained cells were observed in *BHD*-inactivated kidney cells than in control littermates (Fig. 4, D and E). Expression of cell cycle–promoting proteins was also analyzed in *BHD*$^{f/d}$*/KSP-Cre* knockout and littermate control kidneys (Fig. 4, F). Expression of cyclin D1, cyclin A, cyclin B1, cdk4, and cdc2 was higher in *BHD*-inactivated kidneys than in control kidneys, indicating that cells were undergoing rapid proliferation. Cyclin D1 immunohistochemistry revealed strong nuclear staining in dilated tubules of *BHD*-inactivated kidneys (Fig. 4, I and J) but not control kidneys (Fig. 4, G and H), supporting the immunoblotting data that indicated cells lining the dilated tubules were actively proliferating.

To elucidate which signaling pathways were activated by *BHD* inactivation, protein expression levels of several key molecules in pathways involved in cell growth and proliferation were evaluated by immunoblotting (Fig. 5, A). Phospho-c-Raf (Ser338) levels were elevated in kidney lysates from 3-week-old *BHD*$^{f/d}$*/KSP-Cre* mice compared with controls, suggesting that Raf was activated. Consistent with these data, MEK1/2 and Erk1/2, downstream effectors of Raf signaling, and p90RSK, a downstream effector of Erk1/2, were also highly phosphorylated in *BHD*-inactivated kidneys. Immunofluorescence staining of phospho-Erk1/2 in kidney tissue revealed strong specific staining of the dilated tubules in *BHD*-inactivated kidneys (Fig. 5, D and E) but minimal restricted staining in the tubules from control littermates (Fig. 5, B and C).

Activation of another major pathway that is frequently activated in cancer, the PI3K-Akt-mTOR pathway (36,37), was evaluated by immunoblotting (Fig. 6, A). Levels of both total AKT and phospho-Akt (on Thr308) were elevated in *BHD*-inactivated kidneys compared with control kidneys. mTOR was highly phosphorylated at Ser2448 in *BHD*-inactivated kidneys, although total mTOR levels were the same for *BHD*-inactivated and control lysates, consistent with activation of mTOR signaling in *BHD*-inactivated kidneys. Phosphorylation of a downstream effector of mTOR, S6R, on Ser240/244 was also elevated in *BHD*-inactivated kidneys. Immunofluorescence staining for phospho-AKT (Thr 308) revealed membrane staining in some dilated tubules of kidneys in 2-week-old *BHD*-inactivated mice (Fig. 6, D and E) but only restricted staining in kidneys of control mice (Fig. 6, B and C). Phospho-mTOR (Ser2448) staining was seen in all the cells lining the dilated tubules (Fig. 6, H and I), whereas phospho-S6R (Ser234/235) staining was seen in only some cells within the dilated tubules (Fig. 6, L and M). Both proteins were expressed at relatively low levels in control kidneys (Fig. 6, F, G, J, K).

To determine the biochemical consequences of *BHD* inactivation on postnatal kidney development, levels of phosphorylated mTOR were evaluated in kidneys of mice aged from P2 to P21. The staining was identical in control and *BHD*-inactivated kidneys at P2, with strong staining in the developing cortex (Fig. 6, N and R). After 1 week, phospho-mTOR staining in normal tubules was dramatically decreased in control kidneys (Fig. 6, O–Q). However, phospho-mTOR staining was retained in the abnormal dilated tubules from *BHD*-inactivated kidneys during postnatal development (Fig. 6, S–U).

We next asked whether the Akt-mTOR pathway was activated in renal tumors from BHD patients by performing phospho-mTOR (Ser2448) immunohistochemistry. Weak to moderate cytoplasmic staining of phospho-mTOR (Ser2448) was observed in one chromophobe and 13 of 15 oncocytic hybrid tumors from four BHD patients with germline mutations (representative images in Fig. 6, V and W), whereas almost no signal was detected in four normal kidney samples from one non-*BHD* and two BHD patients (Fig. 6, X). These results are consistent with those of another report (38), which described weak phospho-mTOR (Ser2448) staining in sporadic chromophobe renal cell carcinoma and oncocytoma.

One important question that we sought to clarify was whether or not increased cell proliferation in *BHD*-targeted kidneys was through a cell-autonomous mechanism or dependent on environment (ie, stroma). To address this question, we performed primary cell culture of isolated tubule cells from *BHD*-inactivated and control kidneys. *BHD*-targeted kidney cells grew faster in culture than control kidney cells ($P < .001$). Addition of 10 nM rapamycin, which inhibits mTOR, to the culture medium suppressed the rapid growth of *BHD*-inactivated cells and control cells to the same base level (Fig. 7, A–E). The percentage reduction in the growth due to rapamycin treatment by day 9 was twice as large in the *BHD*-inactivated kidney cells as in the control

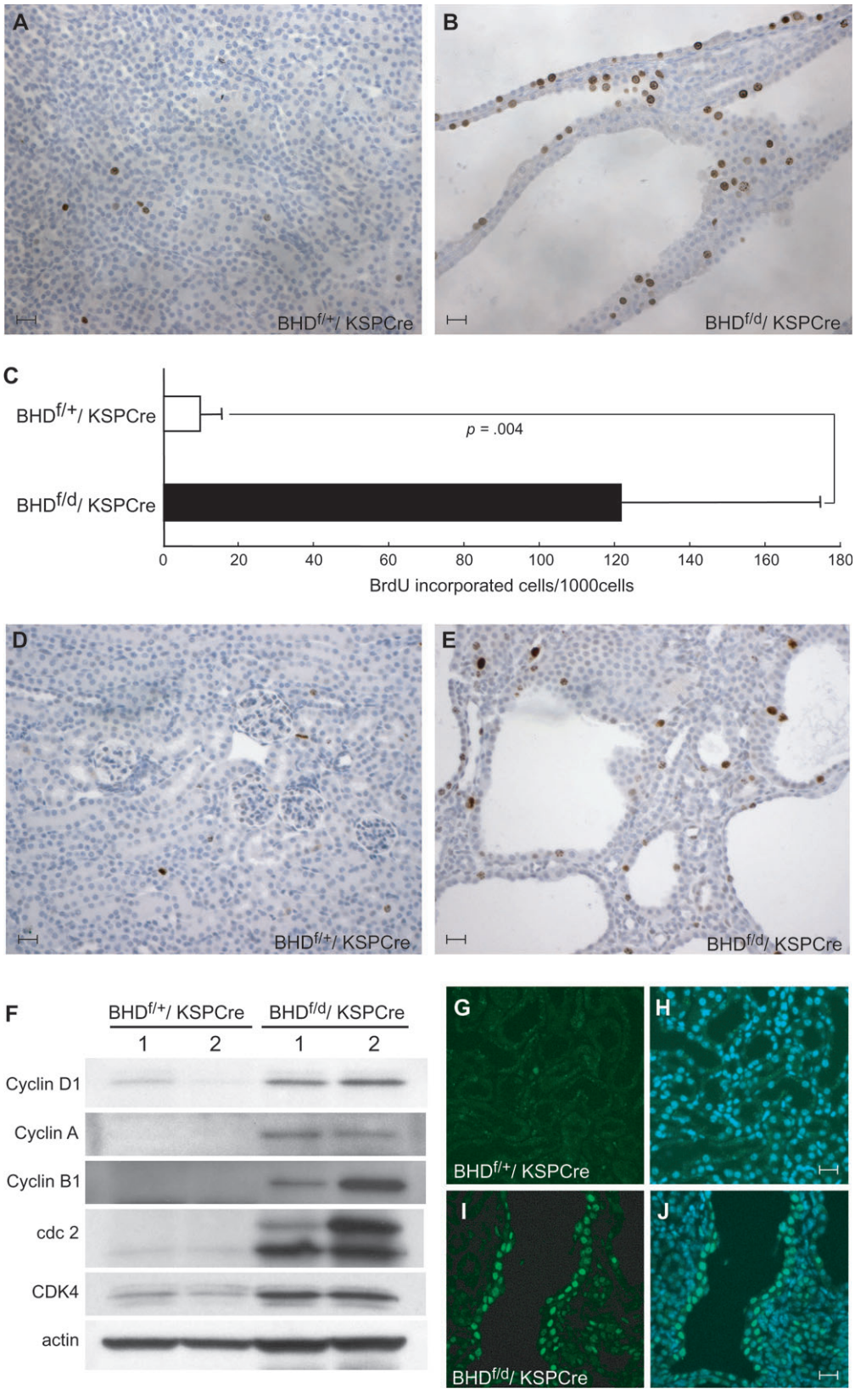

Fig. 4. Evidence of hyperproliferating cells in the kidney of *BHD*$^{f/d}$/*KSP-Cre* mice. 5′-Bromo-2′-deoxyouridine (BrdU) (100 μg/g body weight) was injected intraperitoneally into day (P) 14 *BHD*$^{f/+}$/*KSP-Cre* and *BHD*$^{f/d}$/*KSP-Cre* mice. Two hours later, mice were killed, and kidney samples were subjected to immunostaining to detect BrdU incorporation. **A**) BrdU staining in *BHD*$^{f/+}$/*KSP-Cre* mouse kidney. **B**) BrdU staining in *BHD*$^{f/d}$/*KSP-Cre* mouse kidney. **C**) BrdU incorporation in *BHD*$^{f/d}$/*KSP-Cre* mouse kidneys and *BHD*$^{f/+}$/*KSP-Cre* mouse kidneys. Thousand cells per field were counted in five randomly selected fields from two mice for each group. Data are represented as means and 95% confidence intervals (n = 5 for each group, two-sided *P* value was calculated using Welch's *t* test). **D**) Phospho-histone H3 staining detected few G2/M phase cells in 3-week-old *BHD*$^{f/+}$/*KSP-Cre* kidney. **E**) Phospho-histone H3 staining in 3-week-old *BHD*$^{f/d}$/*KSP-Cre* mouse kidney showed more G2/M phase cells. **F**) Immunoblot analysis of proteins extracted from kidneys of 3-week-old *BHD*$^{f/+}$/*KSP-Cre* and *BHD*$^{f/d}$/*KSP-Cre* mice. Cell cycle–promoting proteins were highly expressed in *BHD*$^{f/d}$/*KSP-Cre* mouse kidneys. Data are representative results for two mice of each genotype from at least three independent experiments. **G**) Weak cyclin D1 staining (**green**) in the kidney of a 2-week-old *BHD*$^{f/+}$/*KSP-Cre* mouse. **H**) Merged image of Cyclin D1 with 4′-6-diamidino-2-phenylindole (DAPI) nuclear staining (**blue**). **I**) Nuclear cyclin D1 staining (**green**) in cells lining the dilated tubules in the kidney of a 2-week-old *BHD*$^{f/d}$/*KSP-Cre* mouse. **J**) Merged image of cyclin D1 with DAPI nuclear (**blue**) staining. **Scale bar** = 20 μm.

kidney cells (17.7% vs 9.1%, difference = 8.6%, 95% CI = 5.1% to 12.0%; $P < .001$).

We also tested whether rapamycin could reverse the cystic kidney phenotype by injecting buffer or rapamycin (2 mg/kg) daily into *BHD*$^{f/d}$/*KSP-Cre* and control mice beginning at P7. Mice were dissected at P21 or before P21, if moribund, and the ratio of kidney to body weight was calculated (Fig. 7, F). Rapamycin treatment did not change the kidney/body weight ratios of control littermates

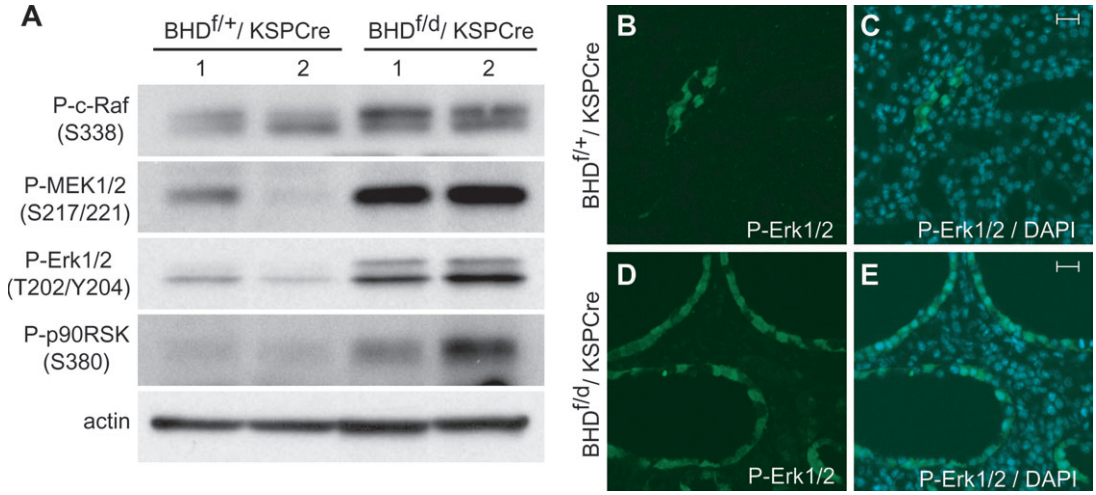

Fig. 5. Activation of Raf-MEK-Erk1/2 signaling pathways in kidneys of *BHD*$^{f/d}$/*KSP-Cre* mice. **A**) Immunoblot analysis of proteins extracted from the kidneys of 2-week-old *BHD*$^{f/+}$/*KSP-Cre* and *BHD*$^{f/d}$/*KSP-Cre* mice. Levels of phospho-c-Raf (Ser338), phospho-mitogen–activated protein kinase (P-MEK) 1/2 (Ser217/221), and phospho-extracellular signal-regulated protein kinase (P-Erk)1/2 (Thr202/Tyr204) were elevated in *BHD* knockout kidneys, as was the level of phosphorylated p90RSK (on Ser380), a downstream effector of Erk. Data are representative results for two mice of each genotype from at least three independent experiments. **B**) P-Erk immunofluorescence staining in control mouse kidneys. **C**) Merged image of P-Erk and 4′-6-Diamidino-2-phenylindole (DAPI) nuclear staining in the control kidney. **D**) Phospho-Erk staining in *BHD* knockout kidneys. **E**) Merged image of P-Erk and DAPI nuclear staining in the kidney of a *BHD* knockout mouse. **Scale bar** = 20 μm.

(buffer vs rapamycin: mean = 0.82% vs 0.88%, difference = 0.06%, 95% CI = –0.11% to 0.24%; $P = .47$), but it reduced the relative kidney/body weight ratio of *BHD* knockout mice at P21 (buffer vs rapamycin: mean = 12.2% vs 4.64%, difference = 7.6%, 95% CI = 5.2% to 10.0%, $P < .001$). Kidneys from buffer-treated *BHD*-inactivated mice showed cystic tubules and ducts characteristic of the *BHD*$^{f/d}$/*KSP-Cre* kidney phenotype, with complete disruption of normal anatomic structures (Fig. 7, G). However, kidneys from rapamycin-treated *BHD*-inactivated mice displayed only mild dilatation of tubules and ducts with retention of some cortical structure at 3 weeks of age (Fig. 7, H).

To examine the effect of rapamycin on survival, *BHD*$^{f/d}$/*KSP-Cre* mice were divided randomly into two groups (n = 4 and n = 5) and injected with buffer or rapamycin (2 mg/kg per day) daily from P7 until mice were found moribund or died. Rapamycin treatment statistically significantly extended the survival period of *BHD*$^{f/d}$/*KSP-Cre* mice (buffer vs rapamycin, median survival: 23 days vs 41.5 days; $P = .0065$) (Fig. 7, I), although all of these mice eventually died from renal failure.

Discussion

In this article, we describe the development of the first conditional *BHD* knockout mouse model in which inactivation of the *BHD* gene is targeted to kidney epithelial cells. Mice with kidney-specific homozygous inactivation of *BHD* exhibited rapid kidney cell proliferation and progressive dilatation of collecting ducts and distal tubules during the first 3 weeks of life with 100% penetrance, which led to severe kidney dysfunction and death. Increased expression of cell cycle proteins and activation of Raf-Erk1/2 and Akt-mTOR pathways were observed in the *BHD* knockout kidneys. Heterozygous *BHD*-targeted littermates displayed a normal phenotype during the study period, suggesting that this dramatic phenotype requires loss of both *BHD* alleles. We found that treatment with the mTOR inhibitor rapamycin reduced kidney size and the extent of tubule dilatation and prolonged survival of the *BHD* knockout mice.

We targeted *BHD* inactivation to the kidney, mainly to the distal nephron, where cadherin 16 is highly expressed (22). However, X-Gal staining of kidneys from mice with the *BHD*$^{f/d}$/*Rosa26LacZ/KSP-Cre* genotype showed mosaic Cre expression in the proximal tubules as well, although the proximal tubules were histologically normal. Only distal tubules and collecting ducts were dilated and cystic in the *BHD* knockout mice, suggesting that *BHD* inactivation produces a phenotype specifically in the kidney cells that make up the distal nephron, consistent with the fact that human *BHD*-associated renal tumors—predominantly chromophobe renal carcinomas and renal oncocytic hybrid tumors—arise from the distal nephron (8). Furthermore, our immunofluorescence staining with vacuolar-H^+-ATPase suggests that in *BHD* knockout mice, intercalated cells of the collecting duct may give rise to the hyperplastic cells with oncocytic-like morphology in the dilated tubules, in agreement with several reports suggesting that intercalated cells may be the origin of chromophobe renal cancer and oncocytoma (33,34). However, although BHD patients have an increased risk for renal cancer, *BHD* knockout mice developed no signs of renal neoplasia before renal failure at 3 weeks, suggesting that additional genetic or epigenetic events are required for progression to neoplasia.

The Raf-MEK-Erk pathway, which is activated in many cancers and regulates cell proliferation (39), was activated in the *BHD* knockout kidneys, consistent with the increased cyclin D1 expression and cell proliferation we observed. Another important regulator of cell growth and protein synthesis, the PI3K-AKT-mTOR pathway (13), was also activated, leading us to hypothesize that a common upstream effector of Raf-MEK-Erk and PI3K-Akt-mTOR pathways (ie, receptor tyrosine kinase) may

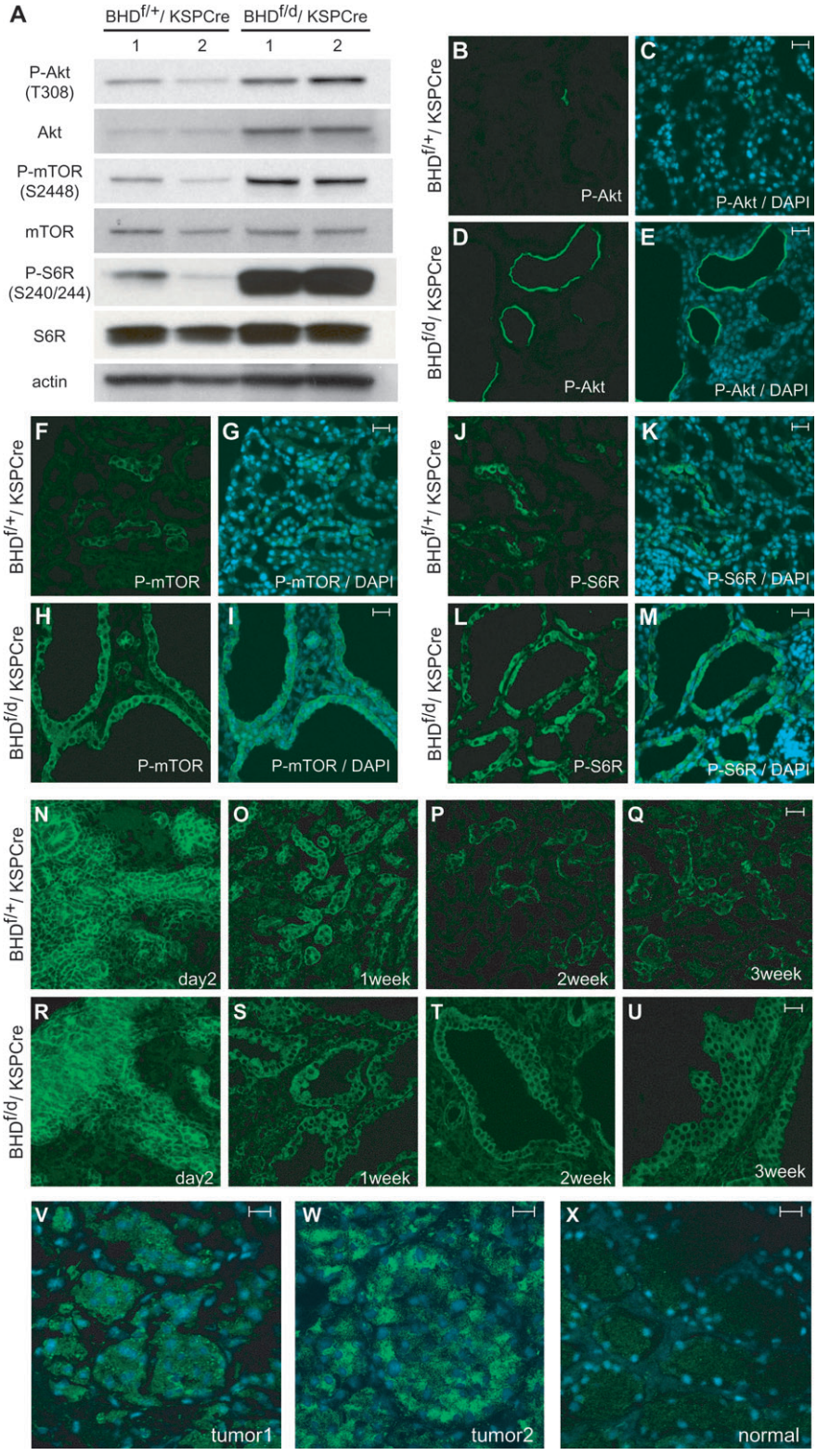

Fig. 6. Activation of Akt/mTOR signaling pathway in kidneys of *BHD*$^{f/d}$/*KSP-Cre* mice. **A**) Immunoblotting analysis of Akt, phosphorylated (P)-Akt (on Thr 308), ribosomal protein S6R, P-S6R (Ser240/244), a measure of activated mammalian target of rapamycin (mTOR), mTOR, and P-mTOR (S2448) in proteins extracted from the kidneys of 3-week-old *BHD*$^{f/+}$/*KSP-Cre* and *BHD*$^{f/d}$/*KSP-Cre* mice. Actin was used as a control for protein loading and transfer. Data represent typical results for two mice of each genotype from at least three independent experiments. P-S6R(235/236) was used for immunofluorescence, and P-S6R(240/244) was used for immunoblots (**B**–**M**) Immunofluorescence staining of P-Akt, P-mTOR, and P-S6R (235/236) in kidneys of 2-week-old control and *BHD* knockout mice. P-Akt staining in the control kidney is very restricted (**B**, **C**). The epithelial cells lining the dilated tubules show membrane staining of P-Akt in *BHD* knockout mouse kidneys (**D**, **E**). Note that not all of the dilated tubules were stained. P-mTOR staining was observed in a small population of tubule cells in control mouse kidneys (**F**, **G**). All dilated tubules in *BHD* knockout mouse kidneys show mTOR phosphorylation (**H**, **I**). P-S6R staining in control mouse kidneys shows restricted staining (**J**, **K**). P-S6R staining in *BHD* knockout mouse kidneys indicates that mTOR is activated in dilated tubules. 4′-6-Diamidino-2-phenylindole (DAPI) nuclear staining (**blue**) is shown (**L**, **M**). (**N**–**U**) P-mTOR staining of kidneys of control and *BHD* knockout mice at different ages. P-mTOR staining in control (**N**) and *BHD* knockout kidneys (**R**) shows identical strong staining patterns in the developing cortex at P2. Fewer tubule cells in kidneys of 1-week-old control mice retain P-mTOR staining (**O**). Tubules in *BHD* knockout mouse kidneys that show dilatation display P-mTOR staining at 1 week (S). At 2 and 3 weeks of age, there are fewer P-mTOR–positive tubules in control mouse kidneys than in *BHD* knockout mouse kidneys (**P**, **Q**). All dilated tubules in kidneys of *BHD* knockout mice at 2 and 3 weeks of age retain P-mTOR staining (**T**, **U**). (**V**–**X**) Renal tumors from BHD patients (representative results from 16 immunostained *BHD* tumor samples) also show P-mTOR staining. P-mTOR staining is seen in the cytoplasm of human BHD patient renal tumor cells (**V**, **W**). Conversely, very little staining is seen in the normal kidney tissue that is adjacent to tumor 1 (**X**). Representative results from four immunostained normal kidney samples are shown. **Scale bar** = 20 μm.

be activated by loss of *BHD* tumor suppressor function, resulting in cell growth and proliferation within the *BHD*-null kidney cell. The rapid growth rate of *BHD*$^{f/d}$/*KSP-Cre* tubule cells in primary culture compared with control tubule cells suggests that this cell proliferation is caused by a cell autonomous mechanism. This mechanism is supported by the fact that *BHD* deletion by KSP-driven Cre recombinase occurred only in kidney epithelial cells, not in stroma, as confirmed by β-galactosidase staining patterns in *BHD*$^{f/d}$/*RosaLacZ*/*KSP-Cre* mice.

As expected, phospho-mTOR (Ser2448) staining of kidney tubules in the developing neonatal kidney of control littermates was evident at birth but gradually declined during the first 3 weeks of life. However, in *BHD* knockout mice, inappropriate phospho-mTOR staining was consistently seen in dilated tubules

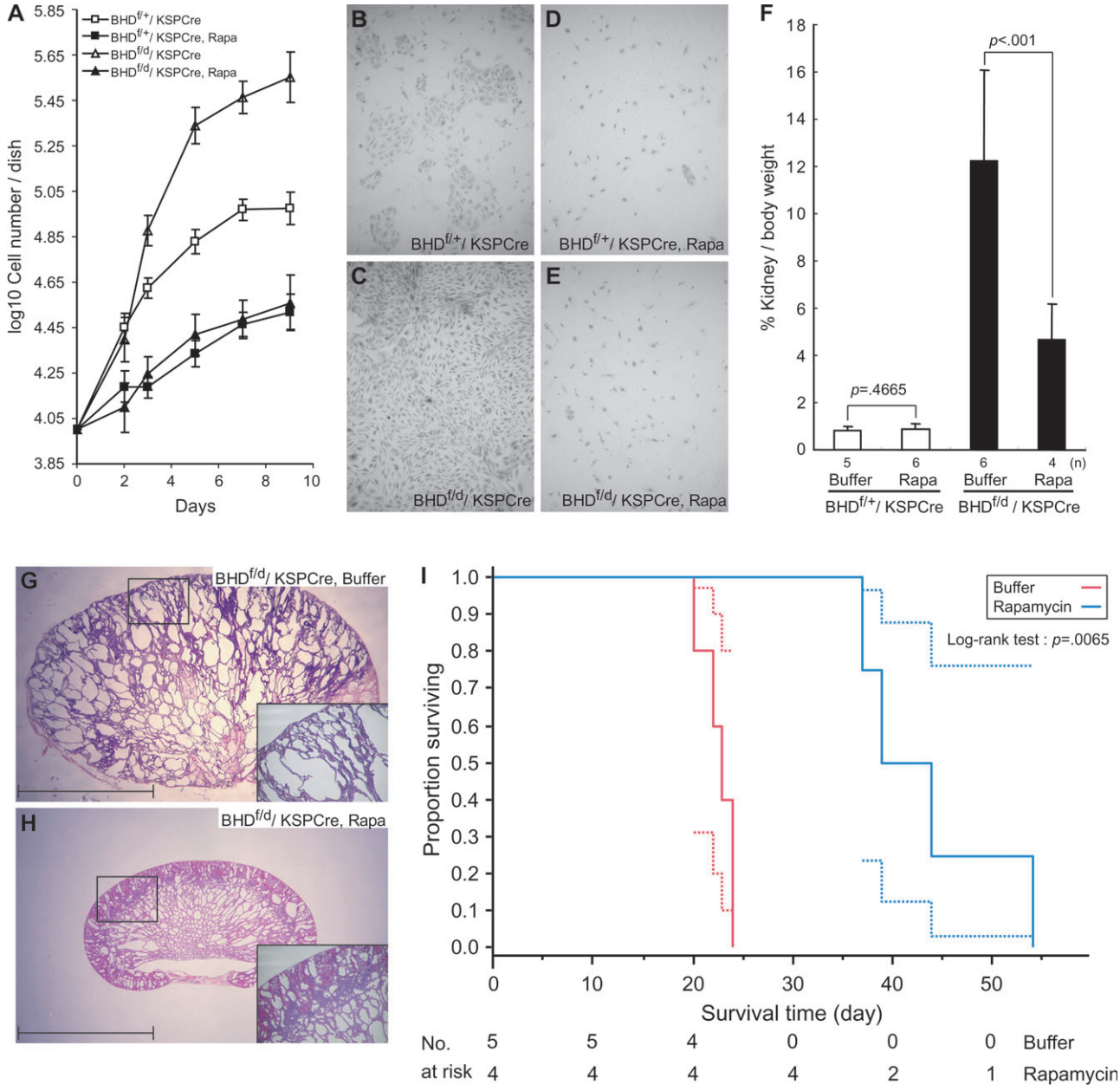

Fig. 7. Effect of rapamycin, inhibitor of mTOR signaling, on *BHD* knockout kidney tubule cell proliferation in vivo and in vitro and on survival of *BHD*$^{f/d}$/*KSP-Cre* mice. **A**) Tubule cells from the kidneys of 3-week-old control (n = 1) and *BHD* knockout (n = 1) mice were isolated, cultured in the presence and absence of rapamycin (10 nM), and counted to evaluate cell proliferation. (**B**–**E**) Representative images of untreated and treated cells from control mice (**B** and **D**) and those of *BHD* knockout mice (**C** and **E**) taken at day 9 are shown. Data are represented as means and 95% confidence intervals (CIs). **F**) Rapamycin (2 mg/kg per day) or buffer was injected into *BHD*$^{f/d}$/*KSP-Cre* and *BHD*$^{f/+}$/*KSP-Cre* mice (*BHD*$^{f/+}$: buffer, n = 5, rapamycin, n = 6; *BHD*$^{f/d}$: buffer, n = 6, rapamycin, n = 4). Mice were dissected at 3 weeks, and relative kidney/body weight ratios (100% × kidney weight/[body weight–kidney weight]) were calculated. Data are represented as means and 95% confidence intervals. *P* values (two-sided) were calculated using the Student's *t* test. **G**) Buffer-treated *BHD*$^{f/d}$/*KSP-Cre* mouse kidneys have numerous cystic tubules and ducts. Inset indicates higher magnification of area in the **square**. **H**) Rapamycin-treated 3-week-old *BHD* knockout mouse kidneys show fewer, less dilated tubules. Inset indicates higher magnification of area in the **square**. **Scale bar** = 5 mm. (**I**) Kaplan-Meier survival analysis show a statistically significant difference between buffer- and rapamycin-treated *BHD* knockout mice. Median survival time of buffer-treated *BHD*$^{f/d}$/*KSP-Cre* mice is 23 days (n = 5) and rapamycin-treated *BHD*$^{f/d}$/*KSP-Cre* mice is 41.5 days (n = 4). Log-rank test (two-sided), *P* = .0065. **Dotted lines**, 95% confidence intervals.

from birth until the mice became moribund at 3 weeks of age, suggesting that *BHD* is necessary for proper regulation of cell growth and proliferation through Akt-mTOR signaling during postnatal kidney development. Our hypothesis that inappropriate Akt-mTOR signaling may have a major role in the enlarged cystic kidney phenotype is supported by the fact that rapamycin treatment dramatically reduced the kidney size and extent of tubule/duct dilatation, caused complete loss of phospho-S6R staining in tubule cells (data not shown), and extended survival of *BHD* knockout mice. In a rat model of autosomal polycystic kidney disease (40), rapamycin treatment reduced both the size of the polycystic kidneys and cystic volume and completely restored kidney function through decrease

in tubular cell proliferation, which is thought to be the first step in cyst formation. Our study also supports tubule cell hyperproliferation as an initiating event of cystic change and rapamycin inhibition of uncontrolled tubule cell growth both in vitro and in vivo.

However, because rapamycin did not completely reverse the cystic kidney phenotype and the *BHD* knockout mice eventually died, other signaling pathways (ie, Raf/Erk, Akt) may contribute to the phenotype caused by loss of FLCN function. Because mTOR inhibition by rapamycin reduces negative feedback to IRS1/2 (41), resulting in Akt activation, the combined treatment of rapamycin and an Akt inhibitor might have a greater effect to suppress uncontrolled cell proliferation in *BHD* knockout mice. Alternatively, kidney cells that have lost FLCN function before P7 may be irreversibly committed to proliferation before initiation of rapamycin treatment at P7.

We previously reported the identification of a novel FLCN-binding partner, FNIP1, that also interacts with AMPK and suggested that FLCN might interact with the AMPK and mTOR signaling pathways through FNIP1 (12). Although in those in vitro studies, which used serum-starved conditions, Akt-mTOR signaling in *BHD*-null tumor cells was slightly elevated relative to that in *BHD*-restored cells, no differences were seen in Akt-mTOR signaling between these two cell lines under normal culture conditions. In contrast, mTOR signaling was inappropriately activated in response to kidney-specific *BHD* inactivation in the mouse. The inconsistencies between the *BHD*-null cell culture data and the *BHD* knockout mouse phenotype underscore the biologic differences between in vitro and in vivo systems and will require further experimentation for clarification.

The obvious limitation of this study is the use of mice to model human disease. Mouse models of human cancer do not always recapitulate the human cancer phenotype, as is also the case for the *BHD* knockout mouse model. Although we have succeeded in inactivating both copies of the *BHD* gene in mouse kidney epithelial cells, the highly cystic kidneys did not develop frank renal neoplasms before renal failure and death. Inactivation of both *BHD* alleles in a human BHD patient kidney cell leads to renal tumorigenesis, but additional unknown genetic events (not introduced in the *BHD* knockout mouse) may occur for kidney tumor development and progression. We were encouraged by the partial response to rapamycin treatment seen in the *BHD* knockout mice but cannot rule out the possibility that other pathways may have been affected by *BHD* inactivation and that the *BHD* knockout mouse may be more effectively treated by combination drug therapy.

In conclusion, we have developed a kidney-specific *BHD*-targeted mouse model that displays a marked polycystic phenotype within the first 3 weeks of life. In this model, homozygous inactivation of *BHD* results in abrupt, uncontrolled cell proliferation, supporting the idea that loss of *BHD* tumor suppressor function may be the first event in multistep renal carcinogenesis in the mouse (42,43). For the *BHD*-inactivated mouse kidney cell to progress to a neoplasm, we hypothesize that additional genetic or epigenetic events may be required to give the *BHD*-null cell a growth advantage and to facilitate progression to renal carcinoma. Indeed, multistep renal cancer progression is suggested by the presence of regions of benign "oncocytosis" adjacent to oncocytic-hybrid tumors in the kidneys of BHD patients (8). Because *BHD*-targeted mice develop a striking kidney phenotype over a very short time, this model may be useful for the development and testing of new therapies or drugs (eg, rapamycin) with which to treat BHD patients and BHD-associated kidney cancers, including sporadic chromophobe renal cancer.

References

1. Birt AR, Hogg GR, Dube WJ. Hereditary multiple fibrofolliculomas with trichodiscomas and acrochordons. *Arch Dermatol.* 1977;113:1674–1677.
2. Toro JR, Glenn GM, Duray PH, et al. Birt-Hogg-Dube syndrome: a novel marker of kidney neoplasia. *Arch Dermatol.* 1999;135:1195–1202.
3. Zbar B, Alvord WG, Glenn GM, et al. Risk of renal and colonic neoplasms and spontaneous pneumothorax in the Birt-Hogg-Dube syndrome. *Cancer Epidemiol Biomarkers Prev.* 2002;11:393–400.
4. Nickerson ML, Warren MB, Toro JR, et al. Mutations in a novel gene lead to kidney tumors, lung wall defects, and benign tumors of the hair follicle in patients with the Birt-Hogg-Dube syndrome. *Cancer Cell.* 2002; 2:157–164.
5. Khoo SK, Giraud S, Kahnoski K, et al. Clinical and genetic studies of Birt-Hogg-Dube syndrome. *J Med Genet.* 2002;39:906–912.
6. Schmidt LS, Nickerson ML, Warren MB, et al. Germline *BHD*-mutation spectrum and phenotype analysis of a large cohort of families with Birt-Hogg-Dube syndrome. *Am J Hum Genet.* 2005;76:1023–1033.
7. Leter EM, Koopmans AK, Gille JJ, et al. Birt-Hogg-Dube syndrome: clinical and genetic studies of 20 families. *J Invest Dermatol.* 2007; 127:1561–1828.
8. Pavlovich CP, Walther MM, Eyler RA, et al. Renal tumors in the Birt-Hogg-Dube syndrome. *Am J Surg Pathol.* 2002;26:1542–1552.
9. Pavlovich CP, Grubb RL 3rd, Hurley K, et al. Evaluation and management of renal tumors in the Birt-Hogg-Dube syndrome. *J Urol.* 2005;173: 1482–1486.
10. Murakami T, Sano F, Huang Y, et al. Identification and characterization of Birt-Hogg-Dube associated renal carcinoma. *J Pathol.* 2007;211: 524–531.
11. Vocke CD, Yang Y, Pavlovich CP, et al. High frequency of somatic frameshift *BHD* gene mutations in Birt-Hogg-Dube-associated renal tumors. *J Natl Cancer Inst.* 2005;97:931–935.
12. Baba M, Hong SB, Sharma N, et al. Folliculin encoded by the *BHD* gene interacts with a binding protein, FNIP1, and AMPK, and is involved in AMPK and mTOR signaling. *Proc Natl Acad Sci USA.* 2006;103: 15552–15557.
13. Inoki K, Corradetti MN, Guan KL. Dysregulation of the TSC-mTOR pathway in human disease. *Nat Genet.* 2005;37:19–24.
14. Corradetti MN, Inoki K, Bardeesy N, DePinho RA, Guan KL. Regulation of the TSC pathway by LKB1: evidence of a molecular link between tuberous sclerosis complex and Peutz-Jeghers syndrome. *Genes Dev.* 2004; 18:1533–1538.
15. Eng CPTEN. one gene, many syndromes. *Hum Mutat.* 2003;22:183–198.
16. Kwiatkowski DJ, Manning BD. Tuberous sclerosis: a GAP at the crossroads of multiple signaling pathways. *Hum Mol Genet.* 2005;14:R1–R8.
17. van Slegtenhorst M, Khabibullin D, Hartman TR, Nicolas E, Kruger WD, Henske EP.The Birt-Hogg-Dube and tuberous sclerosis complex homologs have opposing roles in amino acid homeostasis in schizosaccharomyces pombe. *J Biol Chem.* 2007;282:24583–24590.
18. Lium B, Moe L. Hereditary multifocal renal cystadenocarcinomas and nodular dermatofibrosis in the German shepherd dog: macroscopic and histopathologic changes. *Vet Pathol.* 1985;22:447–455.
19. Lingaas F, Comstock KE, Kirkness EF, et al. A mutation in the canine *BHD* gene is associated with hereditary multifocal renal cystadenocarcinoma and nodular dermatofibrosis in the German shepherd dog. *Hum Mol Genet.* 2003;12:3043–3053.
20. Hino O, Okimoto K, Kouchi M, Sakurai J. A novel renal carcinoma predisposing gene of the Nihon rat maps on chromosome 10. *Jpn J Cancer Res.* 2001;92:1147–1149.
21. Okimoto K, Sakurai J, Kobayashi T, et al. A germ-line insertion in the Birt-Hogg-Dube (*BHD*) gene gives rise to the Nihon rat model of inherited renal cancer. *Proc Natl Acad Sci USA.* 2004;101:2023–2027.
22. Shao X, Somlo S, Igarashi P. Epithelial-specific Cre/lox recombination in the developing kidney and genitourinary tract. *J Am Soc Nephrol.* 2002;13: 1837–1846.

23. Lee EC, Yu D, Martinez de Velasco J, et al. A highly efficient Escherichia coli-based chromosome engineering system adapted for recombinogenic targeting and subcloning of BAC DNA. *Genomics.* 2001;73:56–65.
24. Lewandoski M, Meyers EN, Martin GR. Analysis of Fgf8 gene function in vertebrate development. *Cold Spring Harb Symp Quant Biol.* 1997;62:159–168.
25. Berthet C, Aleem E, Coppola V, Tessarollo L, Kaldis P. Cdk2 knockout mice are viable. *Curr Biol.* 2003;13:1775–1785.
26. Hong S, Furihata M, Baba M, Zbar B, Schmidt LS. Vascular defects and liver damage by the acute inactivation of the VHL gene during mouse embryogenesis. *Lab Invest.* 2006;86:664–675.
27. Copeland NG, Jenkins NA, Court DL. Recombineering: a powerful new tool for mouse functional genomics. *Nat Rev Genet.* 2001;2:769–779.
28. Maquat LE. Nonsense mediated mTNA decay: splicing, translation and mRNP dynamics. *Nat Rev Mol Cell Biol.* 2004;5:89–99.
29. Zolotnitskaya A, Satlin LM. Developmental expression of ROMK in rat kidney. *Am J Physiol.* 1999;276:F825–F836.
30. Takahashi N, Chernavvsky DR, Gomez RA, Igarashi P, Gitelman HJ, Smithies O. Uncompensated polyuria in a mouse model of Bartter's syndrome. *Proc Natl Acad Sci USA.* 2000;97:5434–5439.
31. Shao X, Johnson JE, Richardson JA, Hiesberger T, Igarashi P. A minimal KSP-cadherin promoter linked to a green fluorescent protein reporter gene exhibits tissue-specific expression in the developing kidney and genitourinary tract. *J Am Soc Nephrol.* 2002;13:1824–1836.
32. Lin F, Moran A, Igarashi P. Intrarenal cells, not bone marrow-derived cells, are the major source for regeneration in postischemic kidney. *J Clin Invest.* 2005;115:1756–1764.
33. Storkel S, Pannene B, Thoenes W, Steart PV, Wagner S, Drenckhahn D. Intercalated cells as a probable source for the development of renal oncocytoma. *Virchows Arch B Cell Pathol Mol Pathol.* 1988;56:185–189.
34. Storkel S, Steart PV, Drenckhahn D, Thoenes W. The human chromophobe cell renal carcinoma: its probable relation to intercalated cells of the collecting duct. *Virchows Arch B Cell Pathol Mol Pathol.* 1989;56:237–245.
35. Silve RB, Breton S, Brown D. Potassium depletion increases proton pump (H(+)ATPase) activity in intercalated cells of cortical collecting duct. *Am J Physiol Renal Physiol.* 2000;279:F195–F202.
36. Petroulakis E, Mamane Y, Le Bacquer O, Shahbazian D, Sonenberg N. mTOR signaling: implications for cancer and anticancer therapy. *Br J Cancer.* 2007;96(suppl):R11–R15.
37. Sabatini DM, mTOR. cancer: insights into a complex relationship. *Nat Rev Cancer.* 2006;6:729–734.
38. Robb VA, Karbowniczek M, Klein-Szanto AJ, Henske EP. Activation of the mTOR signaling pathway in renal clear cell carcinoma. *J Urol.* 2007;177:346–352.
39. Roberts PJ, Der CJ. Targeting the Raf-MEK-ERK mitogen-activated protein kinase cascade for the treatment of cancer. *Oncogene.* 2007;26:3291–3310.
40. Tao Y, Kim J, Schrier RW, Edelstein CL. Rapamycin markedly slows disease progression in a rat model of polycystic kidney disease. *J Am Soc Nephrol.* 2005;16:46–51.
41. Shah OJ, Wang Z, Hunter T. Inappropriate activation of the TSC/Rheb/mTOR/S6K cassette induces IRS1/2 depletion, insulin resistance, and cell survival deficiencies. *Curr Biol.* 2004;14:1650–1656.
42. Kinzler KW, Vogelstein B. Lessons from hereditary colorectal cancer. *Cell.* 1996;87:159–170.
43. Kinzler KW, Vogelstein B. Gatekeepers and caretakers. *Nature.* 1997;386:761–763.

Funding

Intramural Research Program, Center for Cancer Research, National Cancer Institute, National Institutes of Health (N01 C012400, P30DK079328 and R01 DK067565 to P.I.).

Notes

We thank Louise Cromwell for excellent technical support with the mouse studies, Mary Ellen Palko for helpful discussions regarding recombineering methodology, and Tim Back for his technical expertise and discussions regarding mouse surgical procedures. We thank Maria Merino for informative, in-depth discussions of comparative human/mouse normal and abnormal histopathology and Octavio Quinones for support in producing some descriptive statistics and graphs and acknowledge the support provided to V. Patel and P. Igarshi by the University of Texas Southwestern O' Brien Kidney Research Core Centre.

The content of this publication does not necessarily reflect the views or policies of the Department of Heath and Human Services, nor does mention of trade names, commercial products, or organizations imply endorsement by the US Government.

The NCI-Frederick is accredited by Association for Assessment and Accreditation of Laboratory Animal Care International and follows the Public Health Service Policy for the Care and Use of Laboratory Animals. Animal care was provided in accordance with the procedures outlined in the "Guide for Care and Use of Laboratory Animals (National Research Council, 1996, National Academy Press, Washington, DC).

Manuscript received July 19, 2007; revised October 24, 2007; accepted November 26, 2007.